Open Access Full Text Article

ORIGINAL RESEARCH

Design and Self-Assembly of Peptide-Copolymer Conjugates into Nanoparticle Hydrogel for Wound Healing in Diabetes

Yiling Lin[1,2], Yingneng Zhang[1,2], Xia Cai[3], Huashen He[2], Chuangzan Yang[2], Junfeng Ban [1,2,4], Bohong Guo[1]

[1]School of Pharmacy, Guangdong Pharmaceutical University, Guangzhou, People's Republic of China; [2]The Innovation Team for Integrating Pharmacy with Entrepreneurship, Guangdong Pharmaceutical University, Guangzhou, People's Republic of China; [3]Guangdong Institute for Drug Control, Guangzhou, People's Republic of China; [4]Guangdong Provincial Key Laboratory of Advanced Drug Delivery, Guangdong Provincial Engineering Center of Topical Precise Drug Delivery System, Guangdong Pharmaceutical University, Guangzhou, People's Republic of China

Correspondence: Junfeng Ban; Bohong Guo, School of Pharmacy, Guangdong Pharmaceutical University, Guangzhou, Guangdong, 51006, People's Republic of China, Tel +86 20 39352309, Email banjunfeng@163.com; bohong-g@163.com

Background: Delayed wound healing in skin injuries has become a significant problem in clinics, seriously affecting and even threatening life and health. Recently, research interest has increased in developing wound dressings containing bioactive compounds capable of improving outcomes for complex healing needs.

Methods: In this study, *Puerarin*-loaded nanoparticles (Pue-NPs) were prepared using the cell-penetrating peptide-poly (lactic-co-glycolic acid) (CPP-PLGA) as a drug carrier by the emulsified solvent evaporation method. Then, they were added into poly (acrylic acid) to obtain a self-assembled nanocomposite hydrogels (SANHs) drug delivery system using the co-polymerization method. The particle size, zeta potential, and micromorphology of Pue-NPs were measured; the appearance, mechanical properties, adhesive strength, and biological activity of SANHs were performed. Finally, the potential of SANHs for wound healing was further evaluated in streptozotocin-induced diabetic mice.

Results: Pue-NPs were regularly spherical, with an average particle size of 134.57 ± 1.42 nm and a zeta potential of 2.14 ± 0.78 mV. SANHs was colorless and transparent with a honeycomb-like porous structure and had an excellent swelling ratio (917%), water vapor transmission rate ($3077 \ \mathrm{g \cdot m^{-2} \cdot day^{-1}}$), mechanical properties (Young's modulus of 18 kPa, elongation at break of 307%), and adhesive strength (15.5 kPa). SANHs exhibited sustained release of Pue over 48h, with a cumulative release of $55.60 \pm 6.01\%$. In vitro tests revealed that the SANHs presented a 92.22% antibacterial rate against *Escherichia coli* after 4h, and a 61.91% scavenging rate of 1.1-diphenyl-2-trinitrophenylhydrazine (DPPH) radical. In vivo experiments showed that SANHs accelerated wound repair by reducing the inflammatory response at the wound site, promoting angiogenesis, and facilitating epidermal regeneration and collagen deposition.

Conclusion: In conclusion, we successfully prepared SANHs. Our results show that SANHs have excellent performance and improves wound healing in diabetic mice model, indicating that it can be used to develop an effective strategy for the treatment of diabetic wounds.

Keywords: *Puerarin*-loaded nanoparticles, nanocomposite hydrogel, drug delivery, wound healing

Introduction

Wound healing is a precise and complex process involving the participation of various cellular and extracellular components, such as bacterial infection and increased exudation, to inhibit granulation tissue formation.[1] Skin is the body's largest organ, and delayed healing of wounds in skin injuries has become a clinical burden, seriously affecting and even threatening life and health.[2,3] Traditional dressings such as gauze can play a passive role in wound healing by masking, absorbing exudates, and preventing injuries from external stimuli. However, the lack of antimicrobial agents or active modulation of endogenous factors to promote wound healing limits their application.[4] Novel nano-formulations

Graphical Abstract
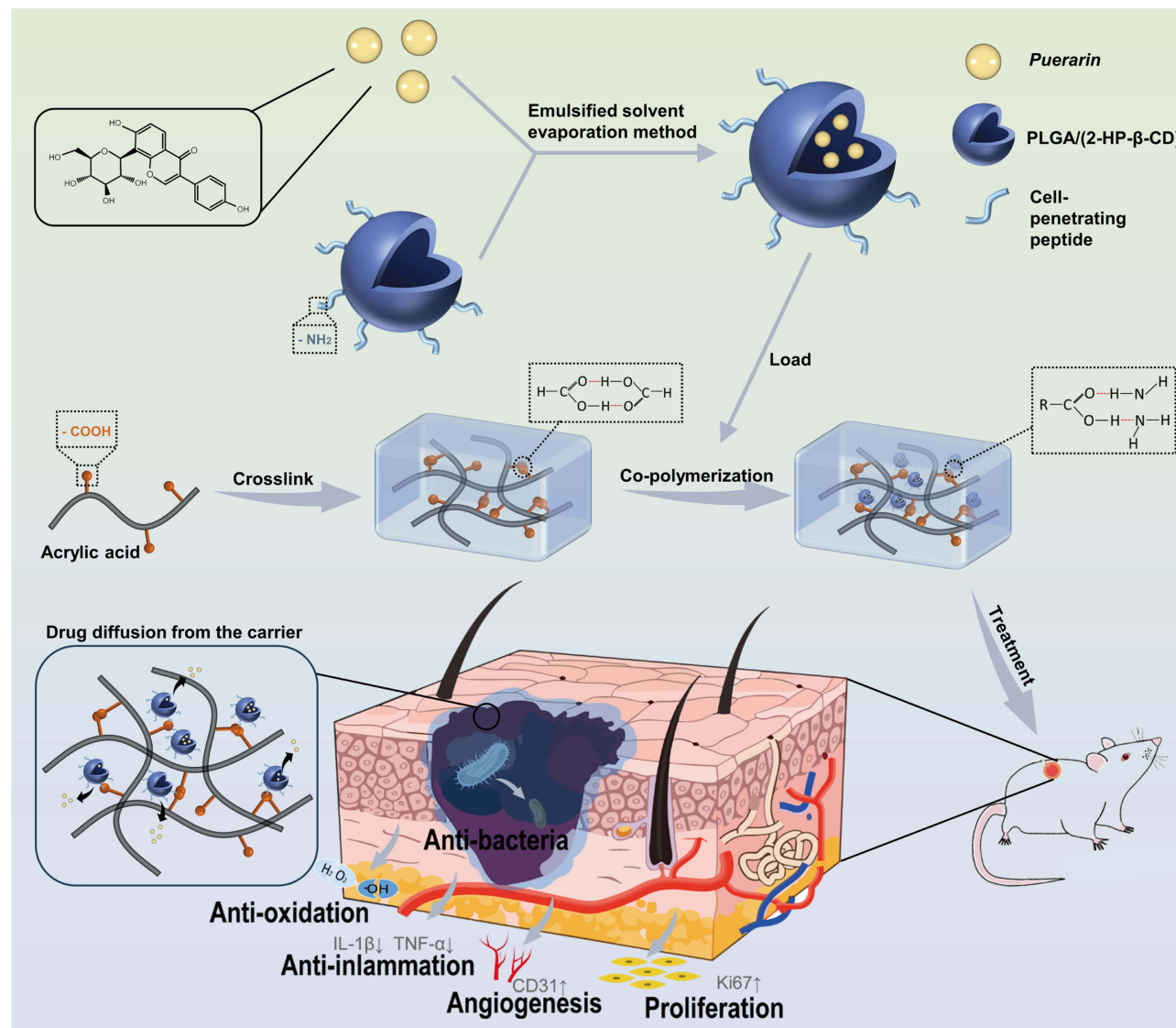
applied in wound healing can enhance the role of endogenous growth factors. Silver nanoparticles with unique physicochemical properties and significant antimicrobial activity can accelerate wound contraction by reducing the bacterial load at the wound site.[5] Zinc oxide nanoparticles are an ideal candidate for carrying pharmacologically active molecules,[6] which can enhance bacterial clearance and stimulate tissue formation.[7] However, such formulations cannot absorb exudates, and make it difficult to adjust the area in response to changes in the wound. Nanocellulose with good biocompatibility, hydrophilicity, and non-toxicity can be applied in humid environments.[8] Mao et al synthesized an in-situ bacterial cellulose/gelatin hydrogel loaded with selenium nanoparticles (BC/Gel/SeNPs), which had saturated solubility up to around 2000% and could be completely degraded in 180 min under the catalysis of cellulase. The loading of nanoparticles resulted in significant antioxidant and antimicrobial capacity. The DPPH radical scavenging rate of BC/Gel/SeNPs was nearly 16 times higher than that of BC/Gel, and the antibacterial activity against four strains of *Escherichia coli* (*E. coli*), *Staphylococcus aureus*, drug-resistant *E. coli*, and drug-resistant *Staphylococcus aureus* was close to 100%. In vivo study found that the composite delivery system could significantly accelerate the wound healing

process, as evidenced by the significantly reduced inflammation and the notably enhanced wound closure, granulation tissue formation, collagen deposition, angiogenesis, and fibroblast activation and differentiation.[9] Therefore, applying bioactive nanoparticles, such as drugs, to wound dressings to accelerate wound healing is a promising strategy.

Hydrogels prepared based on poly(acrylic acid) (PAA) have unique spreading, hydrophilicity, and antibacterial and biocompatibility properties. Shahrousvand et al developed an innovative hydrogel delivery system composed of poly-vinylpyrrolidone/PAA containing ZnO nanoparticles, with multiple properties to facilitate an optimal environment for wound healing. The presence and reasonable distribution of ZnO in the hydrogel structure was observed. Furthermore, due to the loading of ZnO nanoparticles, the inhibitory effect of the system on *Pseudomonas arauginosa* was significantly improved and the wound contraction rate was accelerated on a rat excisional wound injury model.[10] As a wound dressing and effective drug delivery system, PAA hydrogels can maintain inherent bactericidal properties and effectively deliver active drugs to regulate endogenous factors in cells. They provide antibacterial properties of topical drug delivery systems for wounds, with promising application prospects.[11,12]

Puerarin (Pue), a candidate drug compound extracted from the plant *Pueraria lobata*, have strong antioxidant, anti-inflammatory and other pharmacological activities. Previous studies have substantiated that Pue can inhibit oxidative stress by inhibiting ATP production and activating AMPK phosphorylation in a streptozotocin-induced mouse model of type I diabetes,[13] regulate NLRP3 inflammatory vesicles through autophagy, which is protective against hyperglycemia-induced chronic vascular disease,[14] mimic an antibacterial peptide, which kills *E. coli* by binding to lipopolysaccharides and blocking their biological function,[15] and help wound healing by inhibiting NF-κB and MAPK signaling pathways and modulating M2 polarization in macrophages.[16] However, its direct application in wound repair has been limited by low hydrophilicity, poor bioavailability, and low penetration of Pue. Recent research reports suggested that some advanced drug delivery platform, such as nanoparticles, nanofibers and nanogel formulations, can serve as potential carriers for natural products in better management of chronic wound.[17]

In this study, we prepared *Puerarin*-loaded nanoparticles (Pue-NPs) using the cell-penetrating peptide-poly (lactic-co-glycolic acid) (CPP-PLGA) as a drug carrier with the purpose of improving drug bioavailability. To prolong its activity and promote wound healing, a strategy using PAA to form hydrogels (PAA-Gel) and incorporating the Pue-NPs into the PAA-Gel was used to construct a self-assembled nanocomposite hydrogels (SANHs) drug delivery system. The appearance and performances of SANHs were evaluated. We also investigated in vitro antibacterial and antioxidant activities, in vivo wound healing in diabetic mice, and factors involved in its impact on skin tissue repair.

Materials and Methods
Materials
PAA was purchased from Macklin Biochemical Co., Ltd. (Shanghai, China). CPP was manufactured at GL Biochem Co., Ltd. (Shanghai, China). 2-Hydroxypropyl-β-Cyclodextrin (2-HP-β-CD) was bought from Shandong Binzhou Zhiyuan Biotechnology Co., Ltd. (Shandong, China). Polyvinyl alcohol (PVA-0588) was procured from Aladdin Reagent Co., Ltd. (Shanghai, China). Pue was supplied by Shanxi Linzhou Biotechnology Co., Ltd (Shanxi, China). PLGA (LA:GA = 75:25, Mw = 20,000) was bought from Jinan Daigang Biomaterial Co., Ltd. (Shandong, China). Mouse interleukin-1 beta (IL-1β) and mouse tumor necrosis factor-α (TNF-α) ELISA kits were purchased from MEIMIAN (Jiangsu, China). All chemical reagents were of analytical grade.

E. coli (ATCC8739) was gifted from the Guangdong Key Laboratory of Biotechnology Drug Candidate Research Center (Guangdong, China). Male Kunming mice (28–30 days old) were purchased from Guangdong Medical Laboratory Animal Center, license No. SCXK (Guangdong) 2022–0002.

Design and Preparation of SANHs
The preparation process of SANHs comprised two steps. First, Pue-NPs were prepared using the CPP-PLGA as a drug carrier by the emulsified solvent evaporation method. Briefly, 1 g of PVA, 1.5 g of 2-HP-β-CD, and 40 mg of CPP were weighed precisely and dissolved in 100 mL of distilled water to form the aqueous phase. As the organic phase, 40 mg of Pue and 200 mg of PLGA were combined with 5 mL of ethanol and dichloromethane mixed solution ($v{:}v$ = 2:3). Then,

the organic phase was injected slowly into 40 mL of the aqueous phase at 200-W ultrasonic power, 20-kHz frequency, and a phacoemulsification interval of 2 s for 20 min (JYP2-IIdn, Shanghai, China), followed by stirring at a low speed (300 rpm) until the organic solvent evaporated completely. The solution was subsequently increased to a volume of 50 mL with distilled water, after which a microfluidizer high-pressure homogenizer (Nano, Shanghai, China) was used 10 times (25 kpsi, 15°C) to obtain Pue-NPs.

SANHs were further prepared using the co-polymerization method. To be specific, acrylic acid (AA) was mixed with N, N-Methylenebisacrylamide (BIS) that had previously been dissolved in 30% ethanol ($\omega_{BIS}:\omega_{30\%ethanol}$ = 1:40; n_{BIS} :n_{AA} = 2.3%), and the mixture reacted at 60°C in a sealed environment for 1 h to obtain the gel matrix. After the gel matrix cooled to room temperature, Pue-NPs and ammonium persulfate (APS) were added into the system ($n_{APS}:n_{AA}$ = 3.2%; $\omega_{NPs}:\omega_{PAA}$ = 3:7) and reacted at 60°C. The absence of liquid flow indicated the successful preparation of SANHs. Poly(acrylic acid) hydrogels (PAA-Gel) were also prepared to be used as a blank control group (without Pue-NPs).

Characterization and Evaluation of SANHs

Nanoparticles Properties

The particle size distribution, polydispersity index (PDI), and zeta potential properties were determined to verify the properties of Pue-NPs in SANHs using the Delsa Nano C/Zeta potential analyzer (Beckman, California, CA, USA). NPs were directly diluted with water 10 times, and the emission scattering intensity was adjusted to $10,500 \pm 1500$ cps for measurement.

Morphological Features

The microscopic characteristics of Pue-NPs were observed using a transmission electron microscopy (TEM, Tecnai G2 Spirit, Thermo FEI, USA). A drop of nanoparticles solution was pipetted on a copper grid covered with a carbon film; after 5 min of contact, negative staining was performed with 2% phosphotungstic acid solution for 2 min. After the copper grid dried, the surface morphology of Pue-NPs was observed and photographed under an accelerating voltage of 120 kV. The internal structure of SANHs was characterized under a scanning electron microscope (SEM, Gemini SEM300, Carl Zeiss, Germany). SANHs were first dehydrated with liquid nitrogen and broken to obtain cross-sections. The samples were placed on the sample stage, and the holder was sprayed with gold for 60s; then, a current of 10 mA was used to obtain the scanned image.

Swelling Behavior

The degree of swelling of hydrogels is not only affected by its own structure and the ionic strength of the media,[18] but also by environmental conditions such as temperature and pH in contact with the wound.[19] A low swelling ratio cannot ensure complete absorption of wound exudate, and excessive swelling will easily lead to its disintegration. In order to verify the feasibility of SANHs for in vivo studies, we used the weighing method to evaluate the swelling property of SANHs after water absorption. Freeze-dried SANHs were weighed to obtain the initial mass (M_0), followed by immersion in 100 mL of phosphate-buffered solution (PBS) at 37°C. At intervals of 1, 2, 4, 8, 12, 24, 48, and 72 h, SANHs were removed from the solution, and filter paper was used to remove excess water before weighing the sample (M_1). The swelling equilibrium was reached when M_1 did not change anymore. The swelling ratio of SANHs was calculated according to equation (1):

$$\text{Swelling ratio} = \frac{M_1 - M_0}{M_0} \times 100\% \qquad (1)$$

Water Vapor Transmission Rate (WVTR)

WVTR is an important factor affecting the exchange of free water vapor between the skin and the external environment.[20] The ASTM E96 (American Society for Testing Materials) standard approach was used for WVTR measurement with some modifications.[21] Briefly, SANHs were covered over the mouth of a vial containing 12 mL of distilled water, and the connection was sealed with petroleum jelly. Then, the whole unit was placed in a test chamber set at 37°C with 40% relative humidity. The vial was weighed (M_1), and the diameter of the vial's mouth was measured

(2R). The total mass of the vial was reweighed after 24 h (M_2). The WVTR of SANHs was calculated according to equation (2):

$$WVTR\left(g \cdot m^{-2} \cdot day^{-1}\right) = \frac{M_2 - M_1}{2\pi\,R} \qquad (2)$$

Mechanical Properties

Materials used for wound dressings must have specific elasticity, flexibility, and tensile strength properties.[22] The tensile properties of SANHs were assessed using a texture analyzer (TA-XTplus, Stable Micro Systems, UK) equipped with an A/TG probe and a 5-N tension sensor. The SANHs samples were cut into rectangles approximately 50 × 10 mm, the distance between clamping points was 30 mm, and a length of 10 mm was clamped up and down. The stress–strain curves were measured at a speed of 3 mm·min^{-1}. Young's modulus and elongation at break were calculated from stress–strain curves.

Tissue-Adhesive Performance

The structure and composition of the Bama pig organ are more similar to that of human skin; therefore, it is commonly used as a substitute for skin for in vitro evaluation of delivery systems.[23] Fresh porcine skins were selected for lap shear measurement to evaluate the adhesive strength of SANHs. Briefly, the porcine skin was cut into a 10 × 30-mm rectangle and immersed in PBS solution before being used. The prepared SANHs were applied onto the surface of one porcine skin, and two skin sheets were immediately placed face-to-face with an overlap area of 10 × 10 mm (S). After the combination was placed at room temperature for 12 h, the test was carried out by a texture analyzer equipped with a 5-N tension sensor at a speed of 2 mm·min^{-1}. The maximum force value (F_{max}) was recorded at the moment of being pulled apart. The adhesive strength (σ) was calculated according to equation (3):

$$\sigma = \frac{F_{max}}{S} \qquad (3)$$

Spectroscopic Analysis of Pue–Carrier Interactions

An amount of Pue, Pue-NPs, and SANHs was weighed to evaluate the interactions between Pue and carriers in an Fourier-Transform Infrared Spectrometer (FT-IR, Nicolet iS5, Thermo Fisher, New York, USA). The fully dried samples were mixed with potassium-bromide (KBr) at a mass ratio of 1:100, ground, and pressed. Then, the tablets were scanned and analyzed at a wavenumber range of 4000–500 cm^{-1} at room temperature.

A differential scanning calorimetry analyzer (DSC4000, PerkinElmer, USA) was used to analyze the form of Pue in SANHs. About 5 mg of Pue, Pue-NPs, and SANHs were weighed, placed in a standard aluminum pan, and covered. Measurement was performed under a dynamic nitrogen atmosphere (flow rate = 30 mL·min^{-1}) at a constant heating rate of 5°C·min^{-1} at a temperature range of 30–300°C.

The mode of action of Pue with SANHs was further analyzed using an X-ray diffractometer (XRD, Rigaku-SmartLab SE, Tokyo, Japan). The scanning angle was from 5° to 90°, with a scanning speed of 0.01°·s^{-1}, a voltage of 45 kV, and a current of 200 mA.

Encapsulation and Drug Loading Efficiency of SANHs

The Pue content was determined using high-performance liquid chromatography (HPLC, Hclass, Waters, USA). Briefly, an HPLC system with a C18 analytical column was used with a detection wavelength of 250 nm. The mobile phase comprised 18% methanol, 12% acetonitrile, and 70% water. The injection volume, the flow rate, and the column temperature were 10 μL, 1.0 mL·min^{-1}, and 30°C, respectively. The encapsulation efficiency (EE) of NPs was determined by the ultrafiltration-centrifugation method. Pue-NPs (C_3) were centrifuged at a low speed (1000 rpm) for 10 min to separate NPs and the slightly dissolved drug (C_1). The supernatants were transferred into an ultrafiltration tube (with a retention molecular weight of 3 KDa) and then centrifuged at 15,000 rpm for 30 min at 4°C. A small amount of the dissolved drug (C_2) was collected. EE of Pue-NPs was calculated according to equation (4):

$$EE = \frac{C_1 - C_2}{C_3} \times 100\% \tag{4}$$

The loading efficiency (LE) of Pue-NPs was determined by adding an appropriate amount of methanol into the NPs solution to destroy the structure. After being treated with ultrasound for 30 min, the solution was filtered through a 0.22-μm microporous filter membrane for measurement. Similarly, SANHs treated with liquid nitrogen were ground into powder, followed by adding some methanol. The solution was sonicated and filtered as per the above conditions. LE of Pue-NPs and SANHs was calculated according to equation (5):

$$LE = \frac{W_{drug}}{W_{total\ materials}} \times 100\% \tag{5}$$

In vitro Antibacterial and Antioxidant Assay

Antibacterial activity was evaluated by CFU test and SEM method to evaluate the effect of SANHs on bacteria. PAA-Gel, SANHs, and Pue aqueous solution (the content of Pue was the same, 2.4 mg) were prepared and UV-sterilized before the experiment. An *E. coli* bacterial suspension (10^6 CFU mL^{-1}) was added to each sample, and the group without a sample was used as the control. After incubating at 37°C for 4 h, 20 μL of the bacterial suspension was applied to a solid agar plate, incubated for 12 h, and photographed. Then, the viable colonies were counted, and the inhibition efficiency was calculated according to equation (6):

$$\text{Inhibition of} E.coli = \frac{N_C - N_S}{N_C} \times 100\% \tag{6}$$

where N_c and N_s are the bacterial colony counts of the control and sample groups, respectively.

The morphology of the bacteria after different treatments was observed by SEM following a previous report.[24] Bacterial suspensions were treated with 2.5% (*v:v*) glutaraldehyde fixing solution at 4°C overnight, dehydrated using a gradient ethanol aqueous solution, dried at the critical point, and observed.

The antioxidant activity of SANHs was assessed by scavenging the stabilized 1.1-diphenyl-2-trinitrophenylhydrazine (DPPH) radical. PAA-Gel, SANHs, and Pue aqueous solution (the content of Pue was the same, 2.4 mg) were added into 2 mL of ethanolic DPPH solution, and the ethanol solution was used as a negative control. The mixture was incubated for 30 min at room temperature in the dark. Next, using an ultraviolet spectrophotometer, the supernatant was removed to measure the absorbance at 517 nm. DPPH radical scavenging rate was calculated according to equation (7):

$$\text{DPPH scavenging rate} = \frac{A_c - A_S}{A_c} \times 100\% \tag{7}$$

where A_C and A_S are the absorbances of the control and sample groups, respectively.

In vitro *Puerarin* Release Study

The encapsulation of nanoparticles and the porous structure of hydrogels indicate the possibility of slow release of drugs. The in vitro release behavior of Pue-NPs and SANHs was investigated using the dialysis bag method.[25,26] First, different formulations were added into the dialysis bags (with molecular weight cutoff of 8000–14,000 kDa, MYM Biological Technology Company, Limited) and transferred into centrifuge tubes containing 30 mL of PBS at a pH of 7.4. Next, the centrifuge tubes were placed in a constant-temperature shaker at 37°C and 100 rpm. 2 mL of samples were retrieved at intervals of 1, 2, 4, 8, 12, 24, and 48 h. After each interval, the same volume of fresh PBS was supplied. Finally, the samples were filtered through a 0.22-μm membrane filter for the HPLC analysis of the quantity of Pue. Zero-level kinetic, first-level kinetic, Higuchi, and Ritger-Peppas equations were fitted. The cumulative release rate was calculated according to equation (8):

$$X = \frac{\left(C_t \times 25 + V \sum_{i=1}^{t-1} C_i\right)}{m_0} \times 100\% \tag{8}$$

where X is the cumulative drug release at the time point t, m_0 is the total amount of drug added, C_t is the drug concentration at the time point t ($\mu g \cdot mL^{-1}$), C_i is the drug concentration measured at a time point before the t time point ($\mu g \cdot mL^{-1}$), V is the sampling volume (2 mL).

In vivo Diabetic Wound Healing Assessment

Male Kunming mice (18–20 g) were acclimatized under standard conditions, with 12-hour dark/light cycles and food and water ad libitum. According to previous reports,[27] following 12 hours of fasting, an intraperitoneal injection of streptozotocin dissolved in buffered saline (1%, pH = 4.5) at a dose of 140 mg·kg^{-1} body weight was given to the mice to obtain a type I diabetic mice model. Mice with blood glucose levels exceeding 16.7 mmol·L^{-1} for two weeks were diagnosed with diabetes.

Diabetic mice were anesthetized intraperitoneally with 2% pentobarbital sodium solution at a dose of 45 mg·kg^{-1} to construct a wound model. After shaving off the hair from the back of the anesthetized mice with an electric razor and wiping the skin with 0.9% saline, an 8-mm full-thickness skin wound was created using surgical scissors. All the injured mice were randomly assigned to three groups: the model group, the PAA-Gel group and the SANHs group (n = 12/group). The model group was treated with 0.9% saline. Other groups were covered with corresponding hydrogels, which were changed every three days. All the hydrogels were UV-sterilized for 0.5 h before use. Wound areas were photographed and calculated using ImageJ software on days 0, 3, 7, 10, and 14. Orbital blood sampling was performed on mice on days 7 and 14, and serum was obtained from whole blood to determine the expression levels of the inflammatory factors IL-1β and TNF-α using the enzyme-linked immunosorbent assay (ELISA). The wound tissue was collected, fixed with 4% paraformaldehyde, embedded in paraffin, and sectioned. Hematoxylin and Eosin (H&E) staining and Masson's trichrome staining were performed to visualize the pathological changes of the formed tissue and collagen fibers. CD31 and Ki67 immunohistochemical staining was performed to evaluate cell proliferation and vascular remodeling.

Statistical Analysis

The data were collected and analyzed. GraphPad Prism 8.0.2 was used for statistical analysis of the experimental data expressed in means ± standard deviations. Pairwise comparisons were made by a two-tailed Student's *t*-test. One-way ANOVA was used for comparison between multiple groups. The tests revealed no significant differences when $P > 0.05$.

Results and Discussion
Preparation and Characterization of SANHs

CPP-modified polymeric nanoparticles provide an effective means to enhance the intracellular delivery of difficult-to-solve drugs.[28] In this experiment, we first designed and prepared Pue-NPs using CPP–PLGA copolymers as a carrier and then incorporated Pue-NPs into PAA-Gel to achieve bilayer encapsulation of Pue for the long-term treatment of diabetic wounds. As shown in Figure 1A, the obtained Pue-NPs had a clear appearance with light blue and exhibited the "Tyndall effect". TEM images revealed that the morphology of Pue-NPs was regularly spherical, with no adhesion between particles (Figure 1B). The average particle size, PDI, and zeta potential are important parameters, contributing to the stable formation of the nanoparticle solution system. The results presented in Figure 1C and D showed that the average particle size of Pue-NPs was 134.57 ± 1.42 nm, with a PDI of 0.112 ± 0.01 and a zeta potential of 2.14 ± 0.78 mV. In addition, Pue-NPs were stable with no obvious degradation and aggregation after long-term storage.

SANHs can be formed within 2.5 min (Figure 2A). Simple and rapid reaction is the basis for their use in subsequent applications. The prepared SANHs were in a colorless and transparent state. Adding light blue nanoparticles solution did not affect the appearance and shape, making it possible to observe the wound contraction process at any time (Figure 2B). It is worth mentioning that the porous structure of hydrogels facilitated the transport of nutrients and wastes during skin regeneration. The internal morphology of SANHs displayed a honeycomb-like porous structure (Figure 2C), possibly endowing SANHs with sufficient air permeability. Hydrogels prevent wound water loss, providing a moist environment for wound healing. High WVTR can lead to wound dehydration, while too low WVTR causes accumulation and coverage of
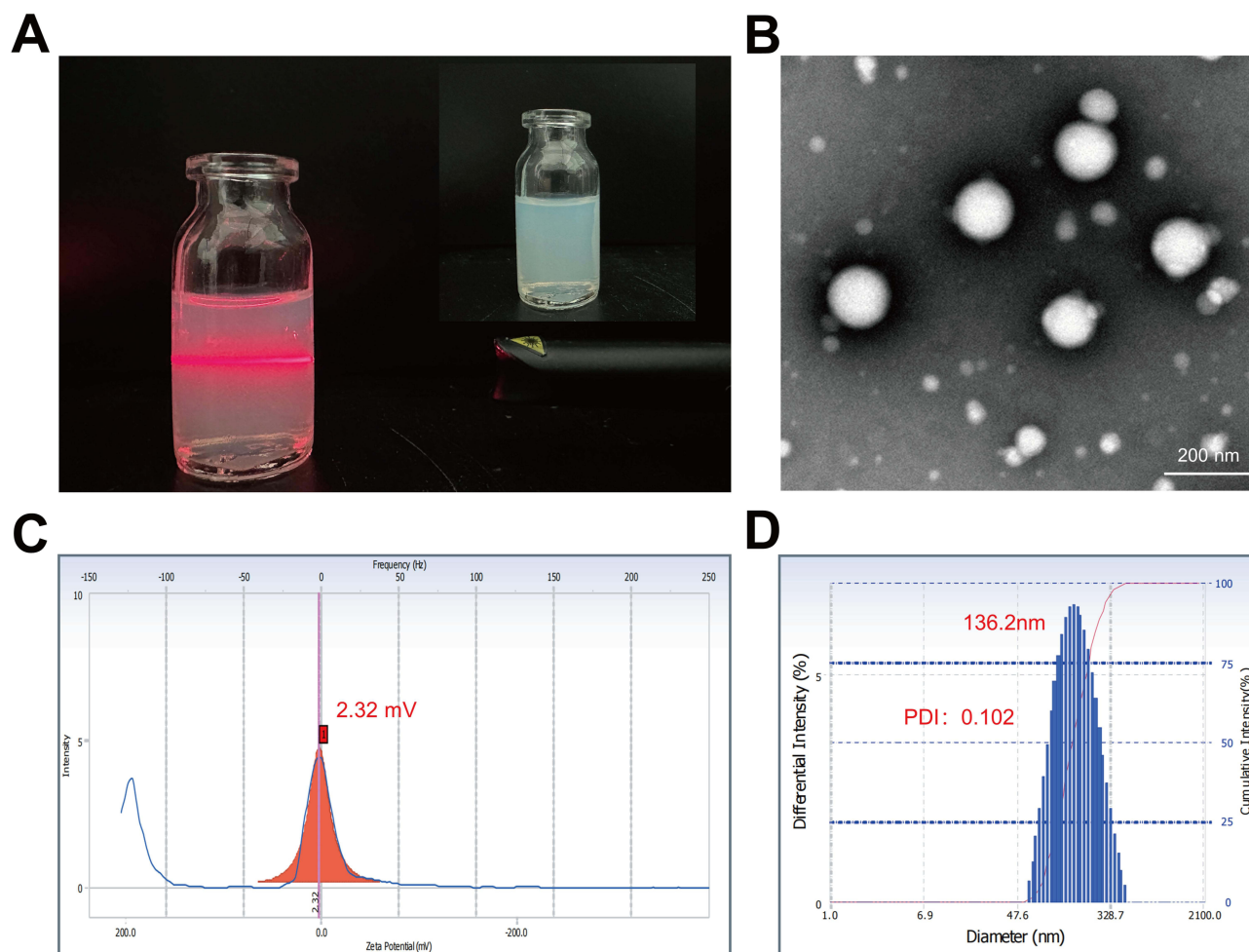
Figure 1 Characterization of Pue-NPs. (**A**) Appearance properties. (**B**) Transmission electron microscope (scale bar: 200 nm). (**C**) Zeta potential. (**D**) Particle size distribution.

wound exudate. It has been reported that the WVTR of an ideal wound dressing is 2000–2500 g·m^{-2}·day^{-1},[29] so we further explored the WVTR of SANHs. Figure 2D showed that the WVTR of SANHs was about 3000 g·m^{-2}·day^{-1}, close to the recommended range of ideal wound dressing. It is well established that hydrogels are characterized by the ability to absorb wound exudate, making us curious to see how effective the swelling of our prepared hydrogels was. As plotted in Figure 2E, the swelling ratio increased dramatically in the first 2 h and reached equilibrium (917%) after 72 h. The equilibrium swelling ratio of SANHs was higher than that of PAA-Gel. We guessed it might be attributed to the decrease of the crosslinking density after loading Pue, and the water was more likely to seep out of the hydrogels. SANHs could absorb the wound exudate quickly in the early stage and maintain a stable shape and volume while preserving a moist healing environment to avoid persistent effects on the surrounding delicate granulation tissue.

Mechanical and Tissue-Adhesive Properties of SANHs

Joints such as ankles, knees, and wrists are mobile and required frequent bending. Therefore, wound dressings are required to have mechanical properties similar to those of skin tissues during the wound-healing process. As shown in Figure 3A, SANHs strips adhered to the finger and adapted well to the finger movement. SANHs could be twisted and bent without deformation and easily peeled off from the finger to ensure no residues, exhibiting their flexible mechanical properties. We further quantitatively tested the mechanical properties of SANHs. Figure 3B suggested that the maximum strain of SANHs was about 320%, which was much higher than the human body can withstand (45–80%).[30] This strong stretchability allowed SANHs to withstand huge deformations and protect the skin tissue. The lower Young's modulus
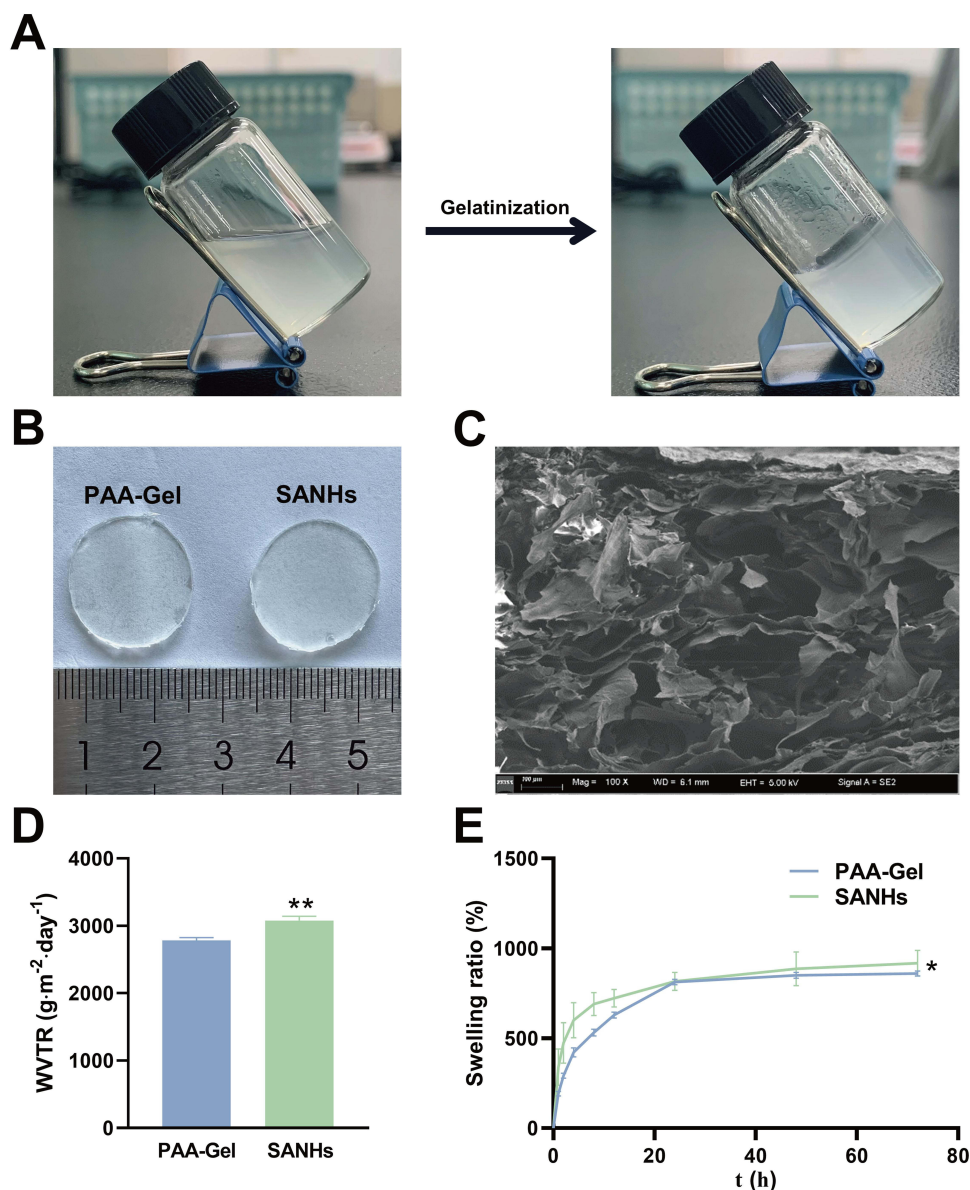
Figure 2 Characterization of SANHs. **(A)** Gelation process. **(B)** Appearance properties. **(C)** Scanning electron microscope (scale bar: 100 μm). **(D)** Water vapor transmission rate. **(E)** Swelling curve (*$P < 0.05$, **$P < 0.01$).

indicate that the hydrogels were softer. Young's modulus of PAA-Gel and SANHs was 69 kPa and 18 kPa (Figure 3C), respectively, within the human skin tissues' range of elasticity modulus (1–100 kPa).[30] The presence of Pue-NPs in SANHs affected the Young's modulus of the system compared to that of PAA-Gel ($P < 0.01$). Furthermore, the elongation at break in the two groups was 307% and 383%, respectively (Figure 3D). The difference after drug loading was probably related to the hydrogen bonds or electrostatic forces between the hydroxyl groups in the molecular structure of NPs and PAA. The binding occurred as a micro-crosslinking, which altered the strength of the crosslinking, and the micro-crosslinked structure acted as a cushioning agent when SANHs were subjected to externally applied forces. In conclusion, adding NPs enhanced the strength and improved the mechanical properties of SANHs, making them more suitable for use as a diabetic wound dressing.

In the first phase of wound healing, excellent adhesion properties of hydrogels enable them to adhere to the wound as a physical barrier to achieve physical hemostasis and provide a favorable healing microenvironment for tissue regeneration. Lap-shear experiments (Figure 3E) were performed on fresh porcine skins to determine the adhesion properties of
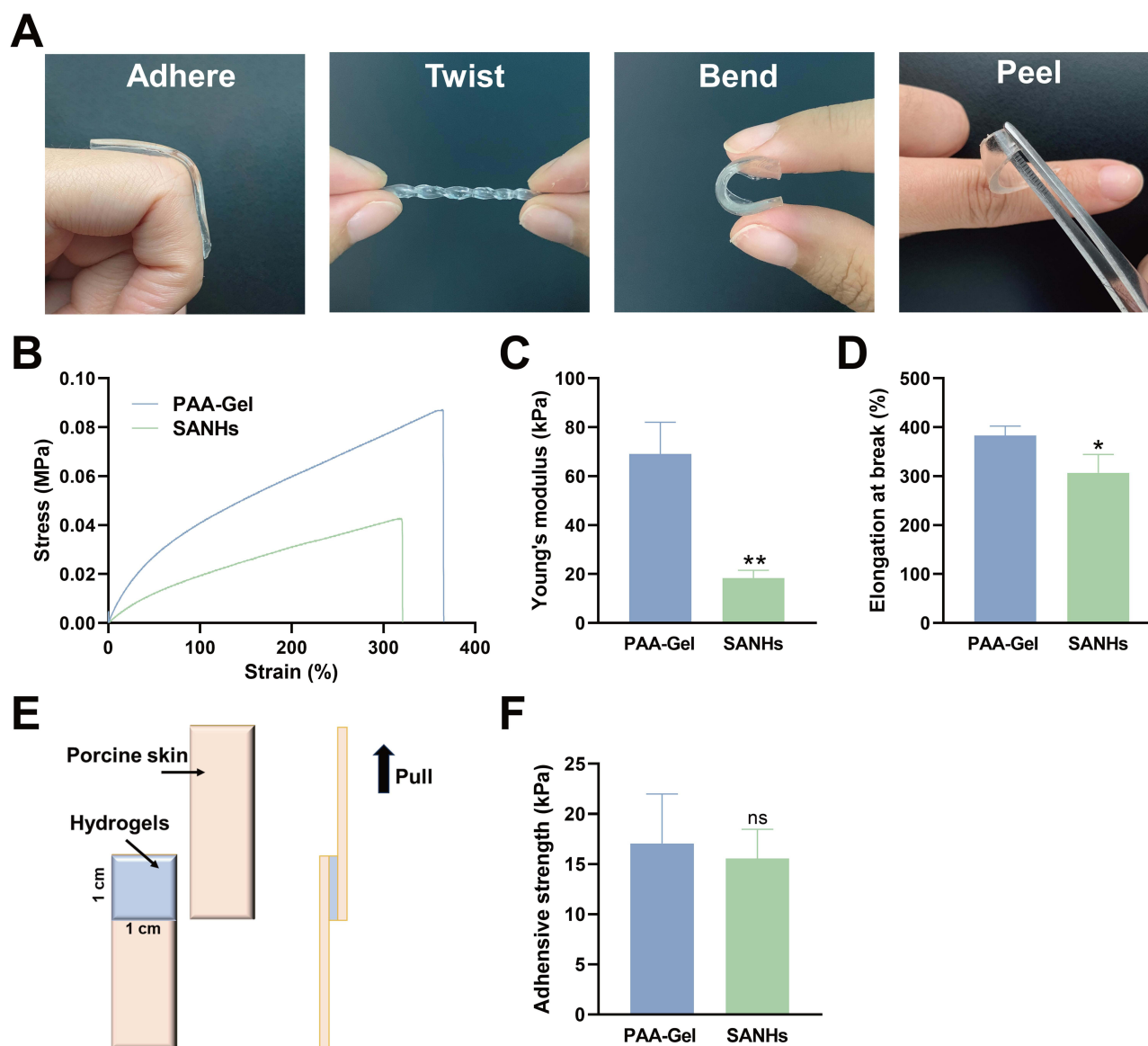
Figure 3 Mechanical and tissue-adhesive properties of SANHs. **(A)** The adhering, twisting, bending, and peeling shapes. **(B)** Stress–strain curve. **(C)** Young's modulus. **(D)** Elongation at break. **(E)** Schematic representation of lap-shear experiments. **(F)** Adhesion strength ($*P < 0.05$, $**P < 0.01$).

SANHs quantitatively. The results (Figure 3F) showed that the adhesion strength of SANHs was 15.5 kPa, nearly three times higher than that of fibrin glue (Greenplast, 5 kPa).[31] The excellent adhesion prolonged the use of SNHHs in the wound, preventing bacterial infection and fluid exudation.

Analysis of Drug Distribution

Figure 4A demonstrates the functional groups of Pue, such as stretching vibration of hydroxyl groups at 3397 cm^{-1}, carbonyl group at 1621 cm^{-1}, and framework vibration of benzene ring at 1609, 1510, 1450 cm^{-1}, as expected and reported previously.[32] However, these characteristic peaks were shifted or disappeared in Pue-NPs and SANHs due to the encapsulation effect. Hydrogen or non-covalent bonds were supposed to form between drugs and excipients, resulting in co-amorphous peaks. XRD patterns (Figure 4B) revealed that Pue had many diffraction peaks at 13.91°, 18.90°, 19.69°, 21.16°, and 23.41° within a certain diffraction angle range (2θ),[33] indicating its crystalline nature. The intensity of the corresponding peaks in Pue-NPs and SANHs decreased significantly, indicating that Pue may exist as molecularly dispersed or in an amorphous state in different formulations. Pue was encapsulated or adsorbed on the surface of the
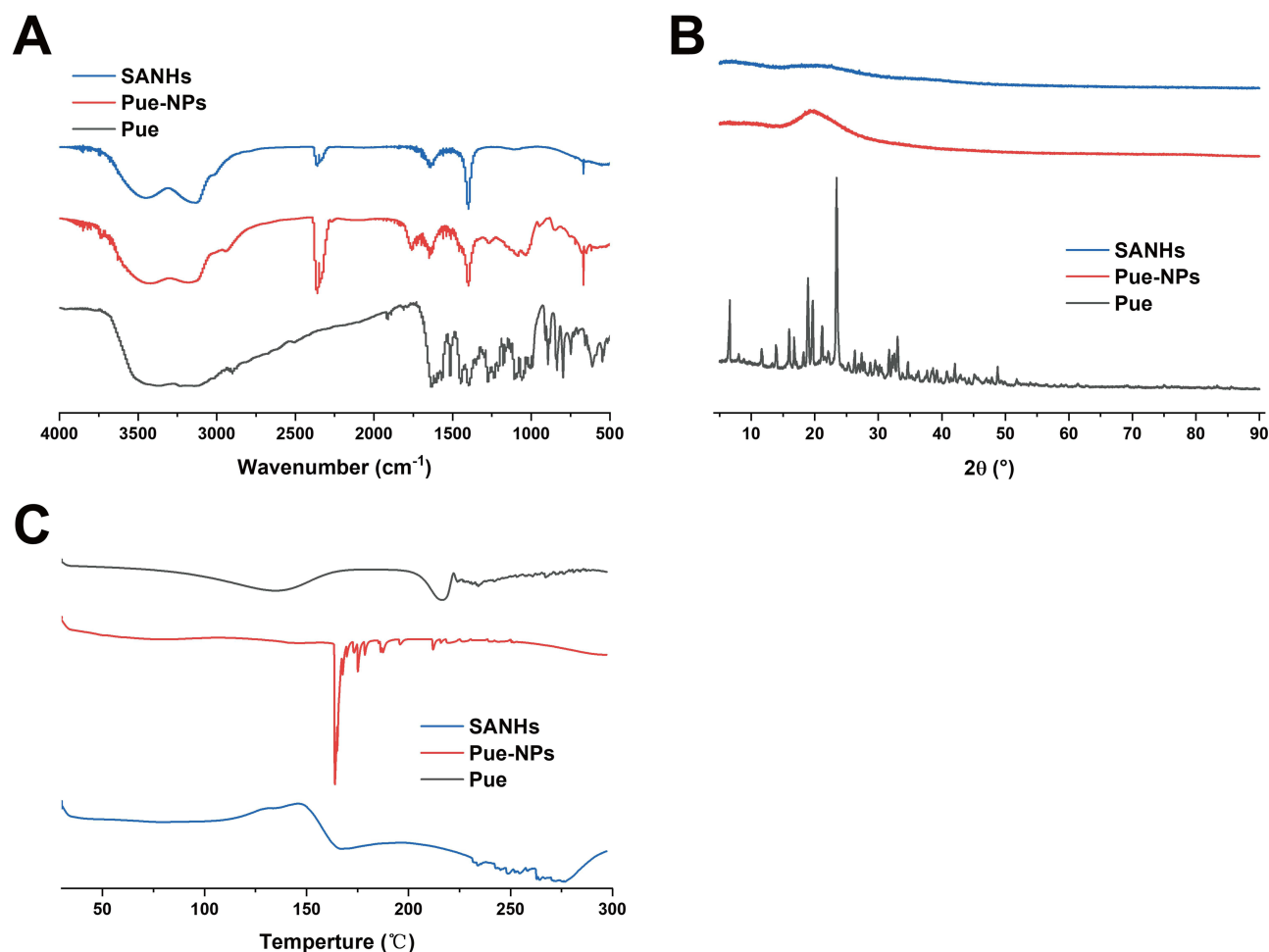
Figure 4 Interaction mode of Pue and carriers. **(A)** Fourier transform infrared spectroscopy spectra. **(B)** X-ray diffraction spectra. **(C)** Differential scanning calorimetry spectra. (Pue, Pue-NPs, and SANHs).

carriers and was no longer purely physically mixed. Crystalline drugs usually have a distinct melting point. Figure 4C depicted the DSC thermogram, revealing that Pue crystals were monohydrates with an endothermic peak due to moisture loss at 135.1°C and a melting peak at 216.4°C.[34] In Pue-NPs or SANHs, the melting peak disappeared, and Pue in the formulations may exist in amorphous or semi-crystalline form.

Analysis of in vitro Drug Release

Before the release behaviors study, the EE% of Pue-NPs was measured at $65 \pm 3.8\%$ by HPLC, and the LE% of Pue-NPs and SANHs was 0.75 ± 0.07 mg·g^{-1} and 0.22 ± 0.02 mg·g^{-1}, respectively. As shown in Figure 5, Pue was released rapidly from Pue-NPs in the first 1 h, with a cumulative release of up to 32.60%. The burst release might be attributed to some free Pue adsorbing onto the surface of the nanoparticles carrier, and its structure was relaxed and rapidly distributed after contact with the release medium.[35] With the degradation of CPP-PLGA, the drug was slowly released, followed by a plateau up to 8 h with a cumulative release rate of 85.98%. The side effects caused by the initial burst release of nanoparticles can affect the stability and safety of drug therapy. In SANHs, Pue-NPs were more tightly bound, and their integrity was well maintained due to the strong interactions between NPs and PAA side chain groups. The cumulative release rate of SANHs was measured at $55.60 \pm 6.01\%$ over 48 h, showing that Pue was released from SANHs in a protracted and sustained manner, attributed to a simultaneous two-step release process. On the one hand, Pue was released from the pore and surface of nanoparticles into the SANHs matrix and then further released outward into the wound tissue. On the other hand, Pue-NPs escaped from SANHs before continuously releasing Pue into the wound
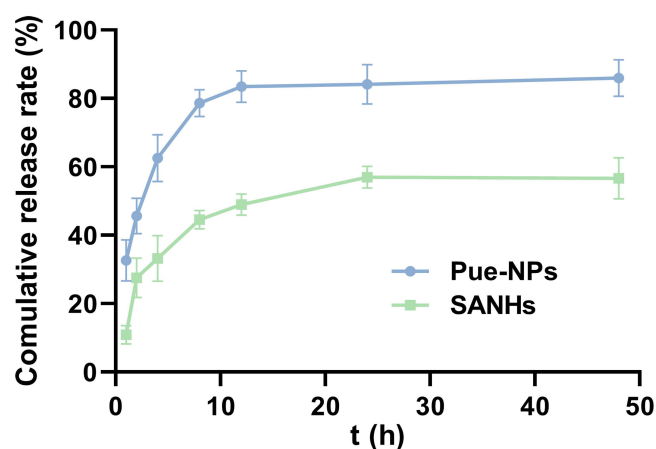
Figure 5 In vitro release curve of Pue-NPs and SANHs in 48 h.

tissue. We fitted the kinetic models for two formulations separately. The fitting results (Table 1) showed that the release of both models was close to the first-order equation, suggesting a correlation between drug release and solution concentration and that the concentration of the drug in the release medium after 48 h had a mitigating effect on the further release of Pue.

In vitro Antibacterial and Antioxidant Efficiencies of SANHs

Diabetic wounds exhibit an extremely high risk of bacterial infection in a high-sugar environment. Although hydrogels can act as a physical barrier to prevent bacterial infection, hydrogels with antimicrobial activity can be a better approach to wound infections by destroying bacteria.[36] Pue has been shown to bind to lipopolysaccharides, which are components of the outer membranes of gram-negative bacteria, to disrupt the bacterial structure and inhibit biofilm formation. It has proved important in preventing infections.[37] This study evaluated the surface antibacterial activity of Pue and SANHs using *E. coli* (gram-negative bacteria). Figure 6A showed the antibacterial activity of PAA-Gel, SANHs, and the same drug content of Pue solution. SANHs were able to produce up to 92.22% bactericidal capacity after 4 h of incubation with the bacterial suspension, which was 2 and 1.2 folds higher than that of Pue solution and PAA-Gel, respectively (Figure 6C). The morphology of the bacteria after different treatments was further observed by SEM, and the results were presented in Figure 6B. The surface of PBS-treated *E. coli* was intact, and the bacteria became slightly crumpled after exposure to the Pue solution. Many wrinkles and disruptions were observed in the SANHs group, suggesting that the

Table 1 Fitting of the in vitro Release Model

| Formulation	Release Model	Equation	R^2
Pue-NPs	Zero-order kinetics	$Q(t) = 0.6688t + 73.0286$	0.1833
	First-order kinetics	$Q(t) = 90.9707(1-e^{-0.5878t})$	0.9556
	Higuchi	$Q(t) = 6.8244t^{1/2} + 59.3560$	0.4285
	Ritger-Peppas	$Q(t) = 60.2261t^{0.1413}$	0.6814
SANHs	Zero-order kinetics	$Q(t) = 0.7453t + 29.3152$	0.5486
	First-order kinetics	$Q(t) = 54.8876(1-e^{-0.2589t})$	0.9489
	Higuchi	$Q(t) = 6.7023t^{1/2} + 18.1858$	0.7728
	Ritger-Peppas	$Q(t) = 21.7619t^{0.2894}$	0.8961
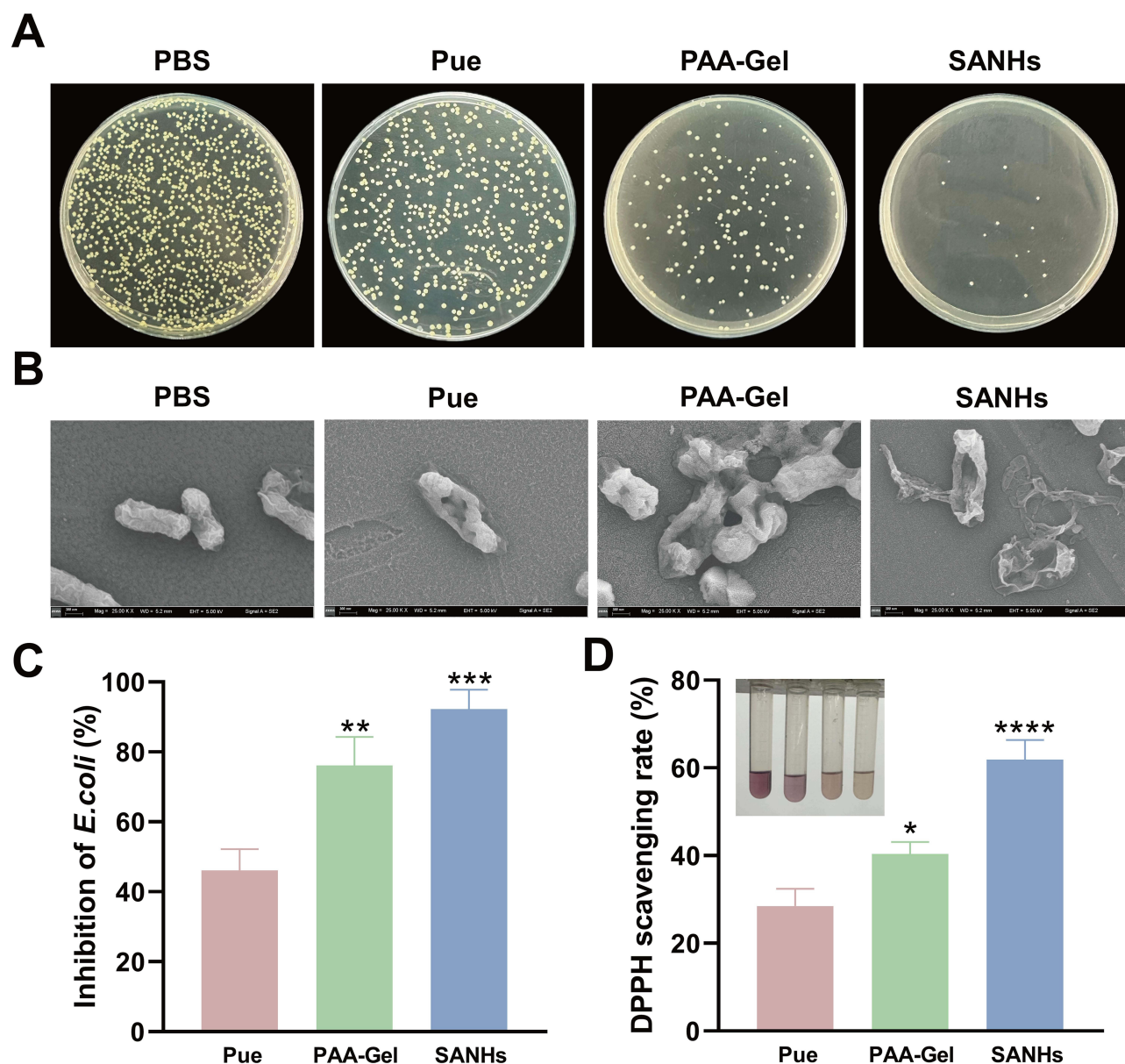
Figure 6 In vitro bioactivity of SANHs. **(A)** Antibacterial properties and **(B)** SEM images of *E. coli* after different treatments. **(C)** Quantification of antibacterial activity. **(D)** Antioxidant properties (*P < 0.05, **P < 0.01, ***P < 0.005, ****P < 0.001).

inhibitory effect of SANHs on *E. coli* was better than the Pue solution. In conclusion, SANHs exhibited excellent antibacterial properties due to the synergistic antibacterial effect of Pue and the hydrogel matrix.

Persistent hyperglycemia and infection lead to excessive accumulation of reactive oxygen species (ROS) in diabetic wounds. At the same time, the activated immune system also produces large amounts of ROS, with all contributing to a significant increase in oxidative stress in the wound environment.[38] Loading antioxidants into hydrogel systems can effectively scavenge ROS, which is an essential step for chronic wound healing. Pue is an excellent free radical scavenger;[39] therefore, it is necessary to evaluate the protective effect in SANHs. The antioxidant activity of SANHs was evaluated by measuring the DPPH radical scavenging rate. The results were presented in Figure 6D. Pue solution with a mass of 2.4 mg and PAA-Gel exhibited scavenging rates of 28.91% and 40.38%, respectively. The antioxidation property of PAA-Gel may be due to the residual initiator in free radical reaction and the high water-retaining property which causing partial ionization of hydrogen ions in carboxyl functional groups. SANHs showed enhanced antioxidant properties (61.91%), suggesting that combining Pue-NPs could effectively enhance the antioxidant activity of SANHs.

In vivo Assessment of SANHs Safety and Effectiveness

Figure 7A summarized the details of establishing and treating diabetic chronic wounds. Representative pictures of wounds and corresponding healing traces in different groups were shown in Figure 7B and C. Macroscopically, the wound areas gradually decreased in size in all the groups, and the SANHs group exhibited faster healing than the other groups at each specific time interval. Notably, after observation for 10 days, the scabs in the SANHs group exfoliated, and hair began to grow around the wounds. The nascent granulation tissues on the wounds were pink and red, while the disease model group was still covered with dry scabs, and the granulation tissues were slow to mature. In addition, the wound area was quantified based on wound photographs to explore the treatment effect (Figure 7D). On days 7, 81.54% wound contraction was achieved in the SANHs group. In comparison, the healing rates were only 65.19% and 73.58% in the disease model and PAA-Gel groups, respectively. By days 14, the wounds of the SANHs group were almost completely repaired, and the healing effect was significantly better than in the disease model and PAA-Gel groups, with statistically significant differences ($P < 0.05$ and $P < 0.005$). However, the disease model group still showed 15.83% of the wound area. The above results indicated that SANHs improved the healing potential of chronic diabetic wounds.

Mice skin tissues were paraffin-embedded, sectioned, and stained with H&E at the end of the experiment to observe the histopathological changes during wound healing. The histological results of the wound site on days 7 and 14 were shown in Figure 8A. On the 7th postoperative day, significant inflammatory infiltrations were observed in the disease model group, indicating a strong inflammatory response at the wound site. In contrast, the SANHs group showed more fibroblasts accompanied by a higher number of blood vessels (green arrows), which provided sufficient nutrients for wound healing. Notably, the SANHs group formed a layer of epithelium (yellow lines), while no epithelialization was seen in the disease model group. On the 14th day, inflammatory cell counts decreased in all the groups, and fewer blood vessels and more skin appendages (hair follicles, blue arrows) appeared in the SANHs group, very similar to the healthy skin tissue. In general, re-epithelialization, the thinning and maturation of epithelial structures, is an important indicator of the degree of skin tissue repair. From days 7 to days 14, the epithelial thickness in the SANHs group tended to thin during the healing process, becoming approximately 76 μm thinner than that in the disease model group (Figure 8C). Since collagen deposition is also an important indicator of the effectiveness of wound healing,[40] collagen deposition density (blue) and alignment of the new skin tissues were evaluated using Masson's trichrome staining (Figure 8B). The results showed that on days 7, the disease model and PAA-Gel groups exhibited muscle fiber accumulation and relatively low collagen content. After 14 days of administration, the collagen content of the three groups was 65.50%, 74.46%, and 82.24% (Figure 8D), respectively, and the SANHs group showed more mature and more closely aligned collagen fibers among all the groups, suggesting an improved extracellular matrix and tissue remodeling. SANHs could promote collagen deposition and correct the abnormal state of deposited collagen fibers, which was conducive to accelerating diabetic wound closure, consistent with the H&E staining results.

IHC staining for CD31 and Ki67 was performed on wound tissue sections on days 7 and 14. Hyperglycemia-induced impairment of endothelial cell function results in abnormal angiogenesis, thus the accelerated angiogenesis positively impacts the reconstruction of skin function in diabetic chronic wounds.[41] As one of the vascular endothelial growth factors, CD31 is an important indicator of neovascularization during wound healing. CD31 protein expression was seen in all the groups (Figure 9A). The quantitative results in Figure 9B show that CD31 in the SANHs group on days 7 and 14 was 3.68% and 6.29% higher than in the model group, respectively. The difference was statistically significant ($P < 0.01$ and $P < 0.005$), suggesting that SANHs effectively accelerated wound repair by promoting angiogenesis. Ki67, a proliferating cell nuclear protein, can be used as a marker to detect the proliferation rate of the cells at the wound site.[42] On days 7, only a small number of Ki67-positive cells were observed in the disease model group. In contrast, extensive cell proliferation was detected in the SANHs group (Figure 9A). On the 14th day, there was a large amount of yellow or brown material accumulation, and the wound site exhibited the highest rate of Ki67-positive cells, which was significantly different from that in the disease model group ($P < 0.005$, Figure 9C), indicating that SANHs effectively accelerated wound closure by promoting cell proliferation. In diabetic wounds, imbalance of inflammatory response regulation induced by macrophages and neutrophils, and an excessive inflammatory response can lead to a difficult transition from inflammation to remodeling period.[16] The expression of inflammatory cytokines IL-1β and TNF-α was further investigated using ELISA (Figure 9D and E). On days 7, IL-1β was released in large
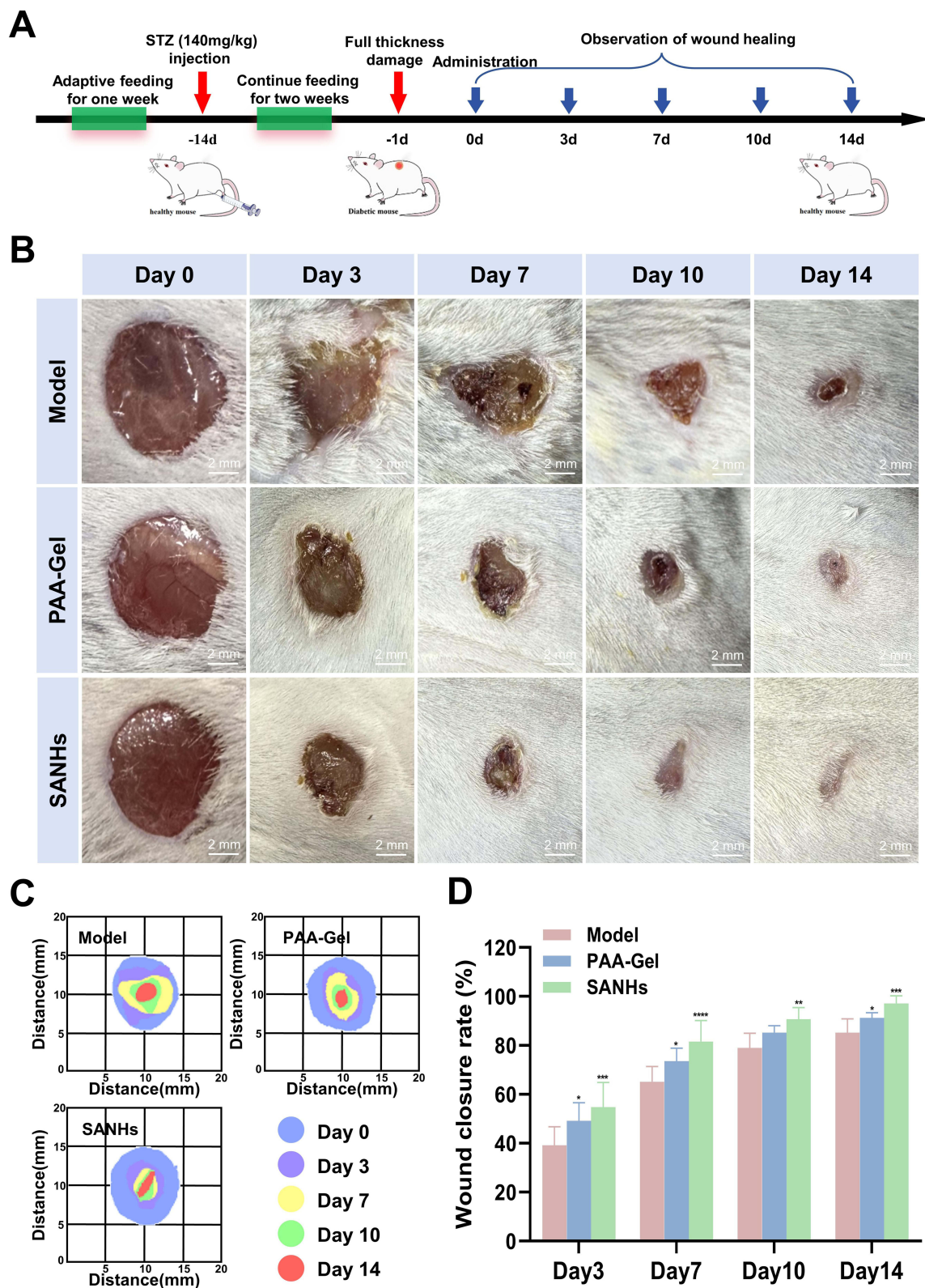
Figure 7 The wound-healing effect of SANHs in a full-thickness skin defect of diabetic mice model. **(A)** The schematic establishment and treatment. **(B)** The wound size on the back of mice on days 0, 3, 7, 10, and 14 after different treatments. **(C)** The corresponding traces and **(D)** wound closure rate of mice after different treatments (*$P < 0.05$, **$P < 0.01$, ***$P < 0.005$, ****$P < 0.001$).
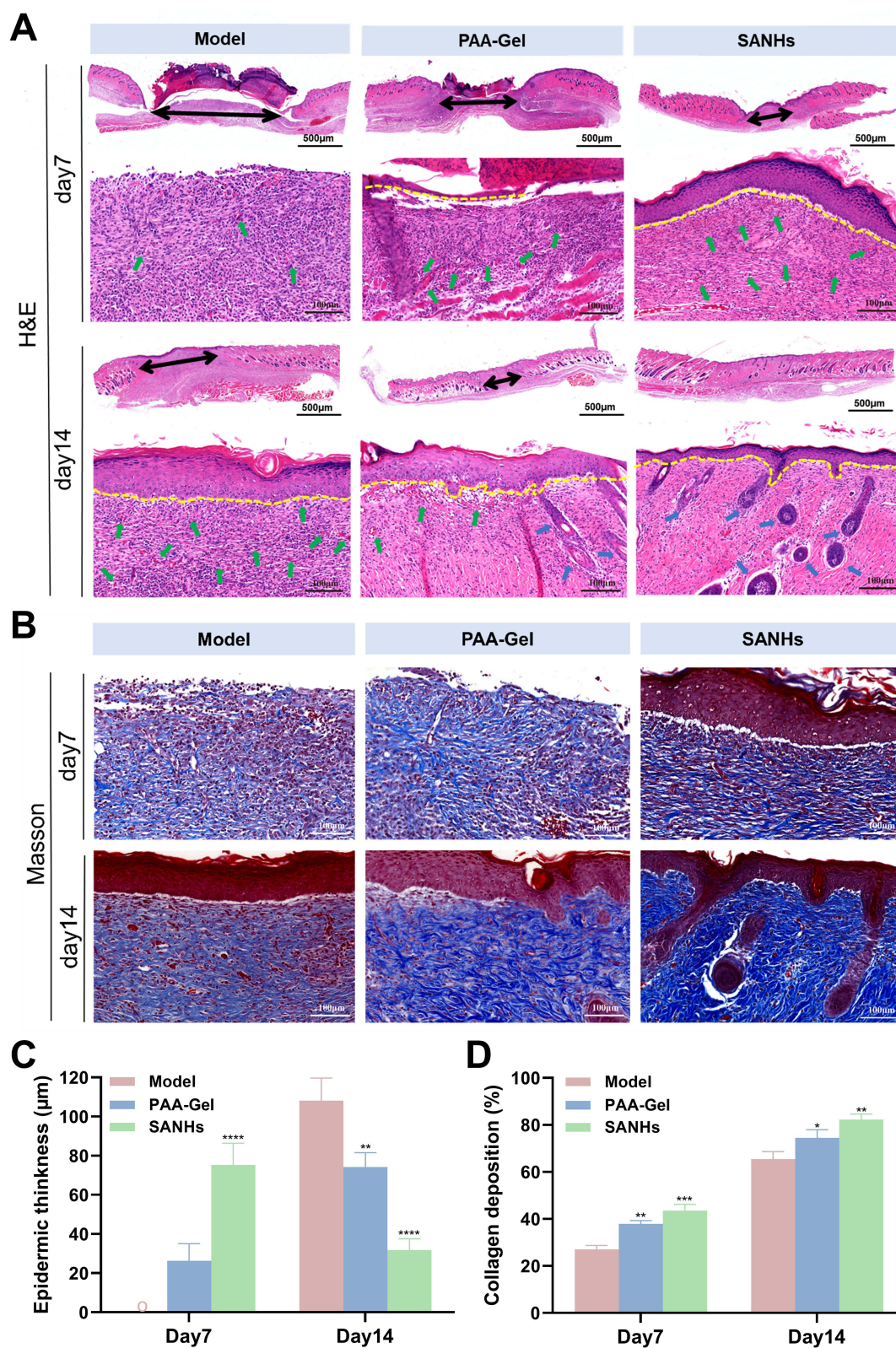
Figure 8 Histopathological analysis of wounds treated with saline (Model), PAA-Gel, and SANHs on days 7 and 14. (**A**) H&E staining. (Yellow lines indicate the boundary between the dermis and epidermis; black, green, and blue arrows represent wound range, blood vessels, and hair follicles, respectively; scale bar: 500 μm and 100 μm). (**B**) Masson's trichrome staining. (scale bar: 100 μm). (**C**) Quantification of epidermic thickness. (**D**) Quantification of collagen deposition (*$P < 0.05$, **$P < 0.01$, ***$P < 0.005$, ****$P < 0.001$).
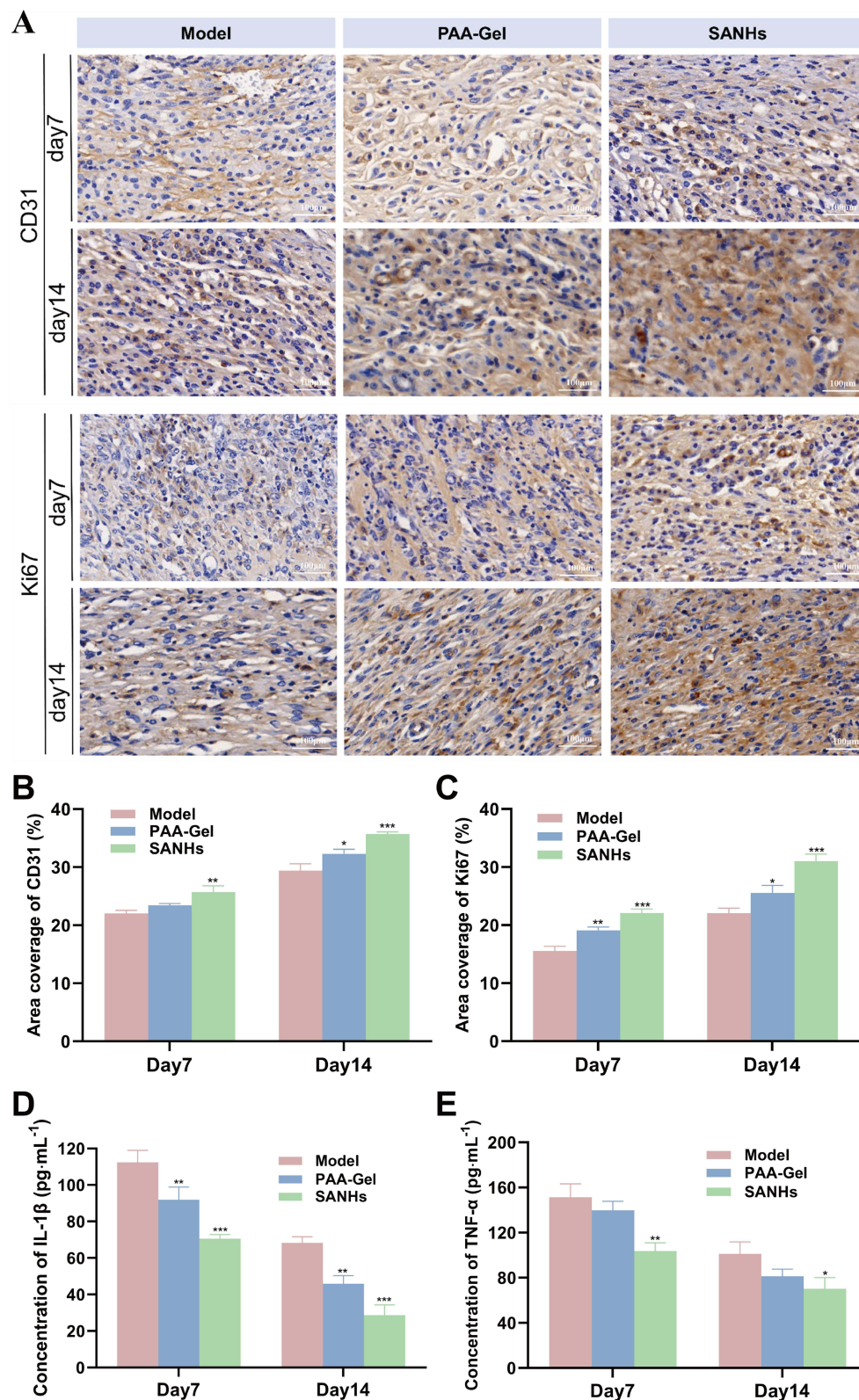
Figure 9 SANHs modulated the microenvironment to promote chronic diabetic wound healing. (**A**) Immunohistochemical detection of CD31 and Ki67 expression in traumatized surfaces on days 7 and 14. Quantitative statistics of the relative area coverage of CD31 (**B**) and Ki67 (**C**). The concentrations of chemokines IL-1β (**D**) and TNF-α (**E**) in wound tissues were determined by ELISA (*$P < 0.05$, **$P < 0.01$, ***$P < 0.005$).

amounts from the lesion area in the disease model group (112 pg·mL^{-1}), which was significantly reduced by SANHs treatment (70 pg·mL^{-1}). Similar results were found for TNF-α: 151 pg·mL^{-1} and 103 pg·mL^{-1} in the model and SANHs groups, respectively. With the subsequent treatment, both IL-1β and TNF-α levels decreased over time in all the groups. In conclusion, SANHs could attenuate the inflammatory response and promote angiogenesis by down-regulating the expression of IL-1β and TNF-α and up-regulating the expression of CD31 and Ki67, thus accelerating wound healing.

Conclusion

Using PAA as a hydrogel matrix, a self-assembled hydrogel co-delivery system (SANHs) was successfully prepared by loading stable Pue-NPs into the hydrogel matrix. The results showed that the distribution of Pue-NPs in SANHs resulted in an exclusive structure, achieving a long-lasting and sustained release of Pue for 48 h and improving the burst release behavior of NPs. Compared with drug-unloaded hydrogels, SANHs exhibited excellent swelling ratio, water vapor permeability, mechanical properties, and tissue adhesion. The presence of NPs increased the antibacterial and antioxidant activity of SANHs. Furthermore, in the study of the mouse diabetes wound model, SANHs showed faster wound healing rate by facilitating epidermal regeneration and collagen deposition. Especially, by upregulating wound healing process related factors (CD31 and Ki67) and reducing production of proinflammatory factor (IL-1β and TNF-α), SANHs promoted cell proliferation and angiogenesis, and reduced the inflammatory response at the wound site. To summarize, combining nanotechnology with hydrogels as a novel drug delivery system provides great potential for the treatment of chronic wound.

Abbreviations

Pue, *Puerarin*; Pue-NPs, *Puerarin* nanoparticles; CPP-PLGA, cell-penetrating peptide-poly (lactic-co-glycolic acid); SANHs, self-assembled nanocomposite hydrogels; PAA-Gel, poly(acrylic acid) hydrogel; 2-HP-β-CD, 2-hydroxypropyl-β-cyclodextrin; PVA, polyvinyl alcohol; WVTR, water vapor transmission rate; DPPH, 1,1-diphenyl-2-trinitrophenylhydrazine; SEM, scanning electron microscopy; TEM, transmission electron microscopy.

Ethics Approval and Informed Consent

The Institutional Animal Care and Use Committee of Guangdong Pharmaceutical University approved the study, ensuring that the care and use of animals conformed to the National Institutes of Health guide for the care and use of laboratory animals (Approval Code: gdpulacspf2022158; Approval Date: 2023-3-24).

Consent for Publication

The authors declare that they have no known competing financial interests or personal relationships that could have appeared to influence the work reported in this paper.

Author Contributions

All authors made a significant contribution to the work reported, whether that is in the conception, study design, execution, acquisition of data, analysis, and interpretation, or in all these areas; took part in drafting, revising or critically reviewing the article; gave final approval of the version to be published; have agreed on the journal to which the article has been submitted; and agree to be accountable for all aspects of the work.

Funding

Disclosure

The authors report no conflicts of interest in this work.

References

1. Wilkinson HN, Hardman MJ. Wound healing: cellular mechanisms and pathological outcomes. *Open Biol*. 2020;10(9):200223. doi:10.1098/rsob.200223
2. Freedman BR, Hwang C, Talbot S, Hibler B, Matoori S, Mooney DJ. Breakthrough treatments for accelerated wound healing. *Sci Adv*. 2023;9(20):76.
3. Zhang W, Liu W, Long L, et al. Responsive multifunctional hydrogels emulating the chronic wounds healing cascade for skin repair. *J Control Release*. 2023;354:821–834.
4. Liang Y, Liang Y, Zhang H, Guo B. Antibacterial biomaterials for skin wound dressing. *Asian J Pharm Sci*. 2022;17(3):353–384.
5. Ahmadi M, Adibhesami M. The Effect of Silver Nanoparticles on Wounds Contaminated with Pseudomonas aeruginosa in Mice: an Experimental Study. *Iran J Pharm Res*. 2017;16(2):661–669.
6. Abebe B, Zereffa EA, Tadesse A, Murthy HCA. A Review on Enhancing the Antibacterial Activity of ZnO: mechanisms and Microscopic Investigation. *Nanoscale Res Lett*. 2020;15(1):190.
7. Saddik MS, Elsayed MMA, El-Mokhtar MA, et al. Tailoring of Novel Azithromycin-Loaded Zinc Oxide Nanoparticles for Wound Healing. *Pharmaceutics*. 2022;14(1):111.
8. Mohammadi S, Jabbari F, Babaeipour V. Bacterial cellulose-based composites as vehicles for dermal and transdermal drug delivery: a review. *Int J Biol Macromol*. 2023;242(Pt 3):67.
9. Mao L, Wang L, Zhang M, et al. In Situ Synthesized Selenium Nanoparticles-Decorated Bacterial Cellulose/Gelatin Hydrogel with Enhanced Antibacterial, Antioxidant, and Anti-Inflammatory Capabilities for Facilitating Skin Wound Healing. *Adv Healthc Mater*. 2021;10(14).
10. Shahrousvand M, Mirmasoudi SS, Pourmohammadi-Bejarpasi Z, et al. Polyacrylic acid/ polyvinylpyrrolidone hydrogel wound dressing containing zinc oxide nanoparticles promote wound healing in a rat model of excision injury. *Heliyon*. 2023;9(8):e19230. doi:10.1016/j.heliyon.2023.e19230
11. Arkaban H, Barani M, Akbarizadeh MR, et al. Polyacrylic Acid Nanoplatforms: antimicrobial, Tissue Engineering, and Cancer Theranostic Applications. *Polymers*. 2022;14(6):1259.
12. Yu H, Sun J, She K, et al. Sprayed PAA-CaO2 nanoparticles combined with calcium ions and reactive oxygen species for antibacterial and wound healing. *Regen Biomater*. 2023;10:rbad071.
13. Hou BY, Zhao YR, Ma P, et al. Hypoglycemic activity of puerarin through modulation of oxidative stress and mitochondrial function via AMPK. *Chin J Nat Med*. 2020;18(11):818–826.
14. Lian D, Liu J, Han R, et al. Kakonein restores diabetes-induced endothelial junction dysfunction via promoting autophagy-mediated NLRP3 inflammasome degradation. *J Cell Mol Med*. 2021;25(15):7169–7180.
15. Yang Y, Chen D, Li Y, et al. Effect of Puerarin on Osteogenic Differentiation in vitro and on New Bone Formation in vivo. *Drug Des Devel Ther*. 2022;16:2885–2900.
16. Li S, Yang P, Ding X, Zhang H, Ding Y, Tan Q. Puerarin improves diabetic wound healing via regulation of macrophage M2 polarization phenotype. *Burns Trauma*. 2022;10:tkac046.
17. Gorain B, Pandey M, Leng NH, et al. Advanced drug delivery systems containing herbal components for wound healing. *Int J Pharm*. 2022;617:121617.
18. Liu G, Lai X, Liu J, et al. Synthesis of a polyacrylamide hydrogel modified with a reactive carbamate surfactant: characterization, swelling behavior, and mathematical models. *Colloids Surf a Physicochem Eng Asp*. 2023;677:132403.
19. Wu L, Wang S, Mao J, Guo Z, Hu Y. Dual network zwitterionic hydrogels with excellent mechanical properties, anti-swelling, and shape memory behaviors. *Eur J Pharm Sci*. 2023;197:112373.
20. Queen D, Gaylor JDS, Evans JH, Courtney JM, Reid WH. The preclinical evaluation of the water vapour transmission rate through burn wound dressings. *Biomaterials*. 1987;8(5):367–371.
21. Pan H, Tang J. Construction of bilayered porous γ-polyglutamic acid/konjac glucomannan hydrogels as potential dressings - ScienceDirect. *Chem Phys Lett*. 2023;830:140823.
22. Zahedi P, Rezaeian I, Ranaei-Siadat S, Jafari S, Supaphol P. A review on wound dressings with an emphasis on electrospun nanofibrous polymeric bandages. *Polym Adv Techs*. 2010;21(2):77–95.
23. Mangelsdorf S, Vergou T, Sterry W, Lademann J, Patzelt A. Comparative study of hair follicle morphology in eight mammalian species and humans. *Skin Res Technol*. 2014;20(2):147–154.
24. Ren G, Huang L, Hu K, et al. Enhanced antibacterial behavior of a novel Cu-bearing high-entropy alloy. *J Mater Sci Technol*. 2022;117:158–166.
25. Han Q, Chen K, Su C, Liu X, Luo X. Puerarin Loaded PLGA Nanoparticles: optimization Processes of Preparation and Anti-alcohol Intoxication Effects in Mice. *AAPS Pharm Sci Tech*. 2021;22(6):217.
26. Li L, Wang L, Luan X, et al. Adhesive injectable cellulose-based hydrogels with rapid self-healing and sustained drug release capability for promoting wound healing. *Carbohydr Polym*. 2023;320:121235.
27. Zhong J, Mao X, Li H, et al. Single-cell RNA sequencing analysis reveals the relationship of bone marrow and osteopenia in STZ-induced type 1 diabetic mice. *J Adv Res*. 2022;41:145–158.
28. Li J, Wei J, Wan Y, et al. TAT-modified tetramethylpyrazine-loaded nanoparticles for targeted treatment of spinal cord injury. *J Control Release*. 2021;335:103–116.
29. Chen X, Wang X, Wang S, Zhang X, Yu J, Wang C. Mussel-inspired polydopamine-assisted bromelain immobilization onto electrospun fibrous membrane for potential application as wound dressing. *Mater Sci Eng C Mater Biol Appl*. 2020;110:110624.
30. Chen X. Making Electrodes Stretchable. *Small Methods*. 2017;1:1600029.
31. Li Y, Yao M, Luo Y, et al. Polydopamine-Reinforced Hemicellulose-Based Multifunctional Flexible Hydrogels for Human Movement Sensing and Self-Powered Transdermal Drug Delivery. *ACS Appl Mater Interfaces*. 2023;15(4):5883–5896.
32. Xie J, Yang F, Shi X, Zhu X, Su W, Wang P. Improvement in solubility and bioavailability of puerarin by mechanochemical preparation. *Drug Dev Ind Pharm*. 2013;39(6):826–835.
33. Li P, Jia H, Zhang S, et al. Thermal Extrusion 3D Printing for the Fabrication of Puerarin Immediate-Release Tablets. *AAPS Pharm Sci Tech*. 2020;21(1):20.

34. Zheng L, Xu H, Hu H, et al. Preparation, characterization and antioxidant activity of inclusion complex loaded with puerarin and corn peptide. *Food Bioscience*. 2022;49:101886.

35. Huang X, Brazel CS. On the importance and mechanisms of burst release in matrix-controlled drug delivery systems. *J Controll Release*. 2001;73 (2):121–136.

36. Qu J, Zhao X, Liang Y, Zhang T, Ma PX, Guo B. Antibacterial adhesive injectable hydrogels with rapid self-healing, extensibility and compressibility as wound dressing for joints skin wound healing. *Biomaterials*. 2018;183:185–199.

37. Ouyang L, Chen B, Liu X, et al. Puerarin@Chitosan composite for infected bone repair through mimicking the bio-functions of antimicrobial peptides. *Bioact Mater*. 2023;21:520–530.

38. Zhao X, Pei D, Yang Y, et al. Green Tea Derivative Driven Smart Hydrogels with Desired Functions for Chronic Diabetic Wound Treatment. *Adv Funct Mater*. 2021;31:2009442.

39. Liu X, Huang R, Wan J. Puerarin: a potential natural neuroprotective agent for neurological disorders. *Biomed Pharmacother*. 2023;162:114581.

40. Wang Y, Ding C, Zhao Y, et al. Sodium alginate/poly(vinyl alcohol)/taxifolin nanofiber mat promoting diabetic wound healing by modulating the inflammatory response, angiogenesis, and skin flora. *Int J Biol Macromol*. 2023;252:126530.

41. Hu Y, Tao R, Chen L, et al. Exosomes derived from pioglitazone-pretreated MSCs accelerate diabetic wound healing through enhancing angiogenesis. *J Nanobiotechnology*. 2021;19:150.

42. Dallas A, Trotsyuk A, Ilves H, et al. Acceleration of Diabetic Wound Healing with PHD2- and miR-210-Targeting Oligonucleotides. *Tissue Eng Part A*. 2019;25(1–2):567.